OPTICAL REVIEW Vol. 7, No. 1 (2000) 25–33

Interferometric Three-Dimensional Imaging Based on Retrieval of Generalized Radiance Distribution

Hidenobu ARIMOTO,[1] Kyu YOSHIMORI[2] and Kazuyoshi ITOH[1]

[1]*Graduate School of Engineering, Department of Applied Physics, Osaka University, 2-1, Yamada-oka, Suita, Osaka, 565-0871 Japan,* [2]*Earth Observation Research Center, National Space Development Agency of Japan, 1-1-9, Roppongi, Minatoku, Tokyo, 106-0032 Japan*

(Received July 14, 1999; Accepted October 27, 1999)

A new three-dimensional (3-D) imaging technique is proposed. The images are obtained as spatial distributions of Walther's first and second definitions of the generalized radiance function. The generalized radiance function can be retrieved from the cross-spectral density measured across an observation plane using a propagation law described in the Fourier domain. The longitudinal resolution of the second generalized radiance function is much higher than that of the first definition, so that the second generalized radiance function is thus useful for the 3-D imaging. Full mathematical descriptions of the principle are given. Results of experimental demonstrations conducted by incorporating uncorrelated two point sources are also reported.

Key words: interferometric imaging, three-dimensional imaging, cross-spectral density, generalized radiance

1. Introduction

The propagation of spatial coherence functions such as cross-spectral density or mutual intensity has recently attracted attention.[1–4] An interferometric imaging technique[5] which is based on measuring the spatial coherence function propagated from sources has also been actively studied.[6–8] The well-known relation between the source intensity distribution and the propagated spatial coherence function is described by the van Cittert-Zernike theorem.[9] According to this theorem, the two-dimensional intensity distribution across a spatially incoherent planar source is proportional to the Fourier transform of the mutual intensity of the paraxial far field. An imaging technique based on the van Cittert-Zernike theorem has long been employed in astronomical observations.[10,11] Unlike these methods that are implemented by measuring the spatial interference fringe, new techniques for obtaining the angular separation or an angular diameter of sources using the spectral interference have also been proposed.[12,13]

These interferometric imaging techniques based on the van Cittert-Zernike theorem are simple and easy to apply to practical observations, however, retrieved images have no information on the source distance. In other words, they are regarded as an image forming system with an infinite focal depth. A principle for three-dimensional (3-D) imaging has thus been needed and new methods were recently proposed.[6,14,15] Using the inverse propagation law of the cross-spectral density described in the four-dimensional Fourier domain, we also proposed a new technique for retrieving the 3-D intensity distribution.[16,17] This distribution is reconstructed by retrieving sequential cross-spectral densities across planes perpendicular to an optical axis unlike most existing methods in which the object image is obtained directly from the measured spatial coherence function. The propagation law of the cross-spectral density in the Fourier domain,[18–20] which plays a central role not only in this technique but also in the principle proposed in this article, has been well known for many years. However, no attempt was ever made to apply this sophisticated representation to 3-D imaging techniques.

In contrast, problems in the relationship between the spatial coherence and radiometry have been investigated for the last three decades.[21] Various definitions of the generalized radiance function (GRF) have been proposed, and theoretical investigations of propagating properties of the radiance dependent upon the source correlation have also been made since Walther first generalized this concept.[22] Walther defined two types of GRFs in his pioneering publications.[22,23]

From this background, we propose a new interferometric 3-D imaging technique based on retrieving the spatial distributions of Walther's GRF. Both the first and the second GRF distributions are retrieved from the measured cross-spectral density across the observation plane that is perpendicular to the optical axis. It is known that Walther's first GRF well conserves along rays particularly in the paraxial resume. Therefore, the first GRF is useful in such as tomography rather than for 3-D imaging. In contrast, conservation of the second GRF is much worse than that of the first except for the limit of short wavelength. The second GRF is thus useful for 3-D imaging. One advantage of this method is the rapidity of required processing. Retrieving the 3-D image by the present method is completed much faster than the method based on retrieving sequential cross-spectral densities.[16,17] A detailed discussion is given in Sect. 4.

The 3-D image is also reconstructed with an image

E-mail: ari@redeye.ap.eng.osaka-u.ac.jp

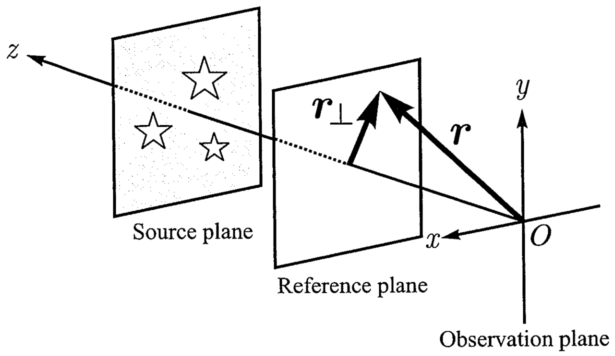

Fig. 1. Geometry of optical system considered.

forming lens by moving the focal point stepwise. However, a large aperture is needed to obtain the higher spatial resolution in such an ordinary image forming system. Moreover, the spectral range is limited to the visible in many cases. On the other hand, a higher resolution can be obtained with a longer two-point separation in the interferometric imaging method, and may be more practicable than using a huge image forming lens. A wide spectral range is also available as seen in radio astronomical observations.

We explain the principle of the 3-D imaging technique by summarizing the propagation law of the cross-spectral density described in the Fourier domain and the relation between Walther's first and second definitions of GRF and the cross-spectral density in Sect. 2. The point spread functions (PSFs) of the proposed imaging technique are also derived. Next, numerically calculated simple examples of GRF images are presented, and differences between the first and second GRFs are discussed in Sect. 3. We report results of experimental demonstrations conducted by incorporating two uncorrelated point sources in Sect. 4. Although Walther's second GRF is originally defined as a real part of the complex radiance function,[19] we also deal with the magnitude of this function. The retrieved 3-D image displayed by the magnitude of the complex radiance function clearly designates the source location compared with that displayed by the real part of the function.

2. Theoretical Foundation

The principle of our imaging technique is based on the propagation law of cross-spectral density in the four-dimensional Fourier domain and the relationship between the cross-spectral density and Walther's radiance functions. These materials are common in literature on radiometry and coherence, so we quickly summarize the relevant part of the theory, which we use to describe the optical system in the geometry illustrated in Fig. 1. We assume planar, quasi-monochromatic light sources in a source plane located at $z=z_s>0$ and an observation plane at $z=0$ which is parallel to the source plane. The origin of the coordinate system is on the observation plane. Let us concentrate our attention on the propagating wavefields toward a negative direction of the z axis in free space. We represent a particular point by a 3-D position vector $\boldsymbol{r}=(\boldsymbol{r}_\perp, z)=(x, y, z)$. Since each plane is perpendicular to the z axis, we represent a location of a point by $(\boldsymbol{r}_\perp, z)$ in the following equations. The space-dependent part of the scalar wavefield $U^{(z)}(\boldsymbol{r}_\perp; \nu)\exp(-2\pi i\nu t)$ satisfies the Helmholtz equation:

$$(\nabla^2+k^2)U^{(z)}(\boldsymbol{r}_\perp; \nu)=0, \tag{1}$$

where ν is the optical frequency, $k=2\pi\nu/c$, and c is the speed of light in free space. At any location, the field may be represented as a Fourier integral:

$$U^{(z)}(\boldsymbol{r}_\perp; \nu)=\iint_{-\infty}^{\infty} \tilde{U}^{(z)}(\boldsymbol{k}_\perp; \nu)\exp(i\boldsymbol{r}_\perp\cdot\boldsymbol{k}_\perp)d^2k_\perp, \tag{2}$$

where $\boldsymbol{k}=(\boldsymbol{k}_\perp, k_z)=(k_x, k_y, k_z)$ is the wavenumber vector. On substituting Eq. (2) into Eq. (1), the following differential equation with respect to $\tilde{U}^{(z)}(\boldsymbol{k}_\perp; \nu)$ is obtained:

$$\left(\frac{\partial^2}{\partial z^2}+k_z^2\right)\tilde{U}^{(z)}(\boldsymbol{k}_\perp; \nu)=0, \tag{3}$$

where

$$k_z=\begin{cases}-[k^2-\boldsymbol{k}_\perp^2]^{1/2} & (k_\perp\le k)\\ -i[\boldsymbol{k}_\perp^2-k^2]^{1/2} & (k_\perp>k).\end{cases} \tag{4}$$

As a solution of Eq. (3), the propagation law of the angular spectrum is represented by

$$\tilde{U}^{(0)}(\boldsymbol{k}_\perp; \nu)=\exp(ik_z z)\tilde{U}^{(z)}(\boldsymbol{k}_\perp; \nu), \tag{5}$$

where $\tilde{U}^{(0)}(\boldsymbol{k}_\perp; \nu)$ is the angular spectrum at the observation plane. According to Eq. (4), the field with $k_\perp>k$ is evanescent. However, we will take only the propagating wave into account. Note that $k_z\le 0$ means that the light propagates toward the negative direction of z since the origin of the coordinate system is on the observation plane.

Next, we consider the cross-spectral density[24] and its propagation law. The cross-spectral density is defined as the cross-correlation of the wavefields at two points $(\boldsymbol{r}_\perp, z)$ and $(\boldsymbol{r}'_\perp, z)$ as

$$W^{(z)}(\boldsymbol{r}'_\perp, \boldsymbol{r}_\perp; \nu)=\langle U^{(z)*}(\boldsymbol{r}'_\perp; \nu)U^{(z)}(\boldsymbol{r}_\perp; \nu)\rangle, \tag{6}$$

where the angular brackets denote the ensemble average and the asterisk denotes the complex conjugate. The four-dimensional Fourier transform of the cross-spectral density with respect to $\boldsymbol{r}_\perp$ and $\boldsymbol{r}'_\perp$ is written as

$$\tilde{W}^{(z)}(\boldsymbol{k}'_\perp, \boldsymbol{k}_\perp; \nu)=\left(\frac{1}{2\pi}\right)^2\iiiint_{-\infty}^{\infty} W^{(z)}(\boldsymbol{r}'_\perp, \boldsymbol{r}_\perp; \nu) \times\exp[-i(\boldsymbol{k}_\perp\cdot\boldsymbol{r}_\perp-\boldsymbol{k}'_\perp\cdot\boldsymbol{r}'_\perp)]d^2r_\perp d^2r'_\perp. \tag{7}$$

Note that we use $\exp[-i(\boldsymbol{k}_\perp\cdot\boldsymbol{r}_\perp-\boldsymbol{k}'_\perp\cdot\boldsymbol{r}'_\perp)]$ for consistency to the related work (See Eq. (5) of Ref. 20)). For convenience of the following explanations, we call the four-dimensional Fourier transform the *angular cross-spectral density*. Equations (2), (6), and (7) lead to another representation of the angular cross-spectral density:

$$\tilde{W}^{(z)}(\boldsymbol{k}'_\perp, \boldsymbol{k}_\perp; \nu)=\langle \tilde{U}^{(z)*}(\boldsymbol{k}'_\perp; \nu)\tilde{U}^{(z)}(\boldsymbol{k}_\perp; \nu)\rangle. \tag{8}$$

On substituting Eq. (5) into Eq. (8), the propagation law of the cross-spectral density from the reference plane to the observation plane is obtained as

$$\tilde{W}^{(0)}(\boldsymbol{k}'_\perp, \boldsymbol{k}_\perp; \nu)=\exp[i(k_z-k'_z)z]\tilde{W}^{(z)}(\boldsymbol{k}'_\perp, \boldsymbol{k}_\perp; \nu). \tag{9}$$

This propagation law of the cross-spectral density represents an exact relationship between $\tilde{W}^{(z)}(\boldsymbol{k}'_\perp, \boldsymbol{k}_\perp; \nu)$ and $\tilde{W}^{(0)}(\boldsymbol{k}'_\perp, \boldsymbol{k}_\perp; \nu)$ since this equation is derived without a paraxial approximation.

Next, we introduce GRF over the reference plane at z. Walther's first GRF[22] is defined by

$$\begin{aligned}
&B^{(z)}_{\mathrm{1st}}(\boldsymbol{r}_\perp, \boldsymbol{s}; \nu)\\
&\quad=|s_z|\left(\frac{k}{2\pi}\right)^2\iint_{-\infty}^{\infty} W^{(z)}(\boldsymbol{r}_\perp-\boldsymbol{\rho}_\perp/2, \boldsymbol{r}_\perp+\boldsymbol{\rho}_\perp/2; \nu)\\
&\qquad\times\exp(-i\boldsymbol{k}_\perp\cdot\boldsymbol{\rho}_\perp)d^2\rho_\perp\\
&\quad=|s_z|\left(\frac{k}{2\pi}\right)^2\iint_{-\infty}^{\infty} \tilde{W}^{(z)}(\boldsymbol{k}_\perp-\boldsymbol{q}_\perp/2, \boldsymbol{k}_\perp+\boldsymbol{q}_\perp/2; \nu)\\
&\qquad\times\exp(i\boldsymbol{q}_\perp\cdot\boldsymbol{r}_\perp)d^2q_\perp,
\end{aligned} \tag{10}$$

where $\boldsymbol{s}=(\boldsymbol{s}_\perp, s_z)=(s_x, s_y, s_z)=\boldsymbol{k}/|\boldsymbol{k}|$. The complex radiance function is defined by

$$\begin{aligned}
B^{(z)}_{\mathrm{c}}(\boldsymbol{r}_\perp, \boldsymbol{s}; \nu)&=|s_z|\left(\frac{k}{2\pi}\right)^2\iint_{-\infty}^{\infty} W^{(z)}(\boldsymbol{r}_\perp, \boldsymbol{r}_\perp+\boldsymbol{\rho}_\perp; \nu)\\
&\qquad\times\exp(-i\boldsymbol{k}_\perp\cdot\boldsymbol{\rho}_\perp)d^2\rho_\perp\\
&=|s_z|\left(\frac{k}{2\pi}\right)^2\iint_{-\infty}^{\infty} \tilde{W}^{(z)}(\boldsymbol{k}_\perp-\boldsymbol{q}_\perp, \boldsymbol{k}_\perp; \nu)\\
&\qquad\times\exp(i\boldsymbol{q}_\perp\cdot\boldsymbol{r}_\perp)d^2q_\perp.
\end{aligned} \tag{11}$$

The real part of the complex radiance function coincides with Walther's original definition of the second GRF.[23] Using Eqs. (7) and (9), the cross-spectral density across an arbitrary transverse plane is retrieved using the measured cross-spectral density across the observation plane, and both the first GRF and the complex radiance function across the arbitrary transverse plane can finally be obtained directly from the measured cross-spectral density:

$$\begin{aligned}
&B^{(z)}_{\mathrm{1st}}(\boldsymbol{r}_\perp, \boldsymbol{s}; \nu)\\
&\quad=|s_z|\left(\frac{k}{2\pi}\right)^2\iint_{-\infty}^{\infty} \tilde{W}^{(0)}(\boldsymbol{k}_\perp-\boldsymbol{q}_\perp/2, \boldsymbol{k}_\perp+\boldsymbol{q}_\perp/2; \nu)\\
&\qquad\times\exp[i\boldsymbol{q}_\perp\cdot\boldsymbol{r}_\perp-i(\kappa^{(+)}_{\mathrm{1st}}-\kappa^{(-)}_{\mathrm{1st}})z]d^2q_\perp,
\end{aligned} \tag{12}$$

and

$$\begin{aligned}
B^{(z)}_{\mathrm{c}}(\boldsymbol{r}_\perp, \boldsymbol{s}; \nu)&=|s_z|\left(\frac{k}{2\pi}\right)^2\iint_{-\infty}^{\infty} \tilde{W}^{(0)}(\boldsymbol{k}_\perp-\boldsymbol{q}_\perp, \boldsymbol{k}_\perp; \nu)\\
&\qquad\times\exp[i\boldsymbol{q}_\perp\cdot\boldsymbol{r}_\perp-i(k_z-\kappa_{\mathrm{c}})z]d^2q_\perp,
\end{aligned} \tag{13}$$

where

$$\kappa^{(\pm)}_{\mathrm{1st}}=-[k^2-(\boldsymbol{k}_\perp\pm\boldsymbol{q}_\perp/2)^2]^{1/2}, \tag{14}$$

and

$$\kappa_{\mathrm{c}}=-[k^2-(\boldsymbol{k}_\perp-\boldsymbol{q})^2]^{1/2}. \tag{15}$$

Retrieved radiance functions reflect the intensity distribution. Let us consider radiance functions for the quasi-homogeneous source.[24] The assumption of quasi-homogeneity implies that the spectral density $S^{(z_s)}(\boldsymbol{r}_\perp; \nu)$ varies much more slowly than the effective correlation length which is characterized by the spectral degree of coherence $\mu^{(z_s)}(\boldsymbol{r}_\perp; \nu)$, and the first GRF at z can then be written by

$$B^{(z)}_{\mathrm{1st}}(\boldsymbol{r}_\perp, \boldsymbol{s}; \nu)=|s_z|\left(\frac{k}{2\pi}\right)^2 S^{(z)}(\boldsymbol{r}_\perp; \nu)\tilde{\mu}^{(z)}(\boldsymbol{k}; \nu), \tag{16}$$

and the complex radiance function by

$$\begin{aligned}
&B^{(z)}_{\mathrm{c}}(\boldsymbol{r}_\perp, \boldsymbol{s}; \nu)\\
&\quad=|s_z|\left(\frac{k}{2\pi}\right)^2\iint_{-\infty}^{\infty} S^{(z)}(\boldsymbol{r}_\perp+\boldsymbol{\rho}_\perp/2; \nu)\mu^{(z)}(\boldsymbol{\rho}_\perp; \nu)\\
&\qquad\times\exp(-i\boldsymbol{k}_\perp\cdot\boldsymbol{\rho}_\perp; \nu)d^2\rho_\perp,
\end{aligned} \tag{17}$$

where $\tilde{\mu}(\boldsymbol{k}; \nu)$ is the two-dimensional Fourier transform of the spectral degree of coherence. Equation (16) is derived under the approximation $[S^{(z)}(\boldsymbol{r}_\perp-\boldsymbol{\rho}_\perp/2; \nu)S^{(z)}(\boldsymbol{r}_\perp+\boldsymbol{\rho}_\perp/2; \nu)]^{1/2}\simeq S^{(z)}(\boldsymbol{r}_\perp; \nu)$. In a special case where the source field is spatially incoherent, both radiance functions across the source plane are proportional to the intensity distribution as follows:

$$B^{(z)}_{\mathrm{1st}}(\boldsymbol{r}_\perp, \boldsymbol{s}; \nu)=B^{(z)}_{\mathrm{c}}(\boldsymbol{r}_\perp, \boldsymbol{s}; \nu)=|s_z|\frac{k^2}{(2\pi)^3}S^{(z_s)}(\boldsymbol{r}_\perp; \nu). \tag{18}$$

Both the first GRF and the complex radiance function are obtained by taking the two-dimensional Fourier transform of the product of the propagation kernel and the angular cross-spectral density of the observation plane. In a practical experiment, the cross-spectral density with respect to all pairs of points $(\boldsymbol{r}'_\perp, \boldsymbol{r}_\perp)$ within the observation area may be measured using a rotational-share interferometer or a wave-front-folded interferometer.[11] Therefore, the four-dimensional Fourier transform of the measured cross-spectral density with respect to $\boldsymbol{r}_\perp$ and $\boldsymbol{r}'_\perp$ must be taken. After taking the Fourier transform, successive applications of Eq. (12) or Eq. (13) by changing z give sequential distributions of the first GRF or the complex radiance function over the x–y–z space. It should be noted that the selected direction of $\boldsymbol{s}$ in Eq. (12) must not be (0, 0, −1) for 3-D imaging because the first GRF is independent of the propagation distance z when $\boldsymbol{s}_\perp=(0, 0)$. This implies that the first GRF with respect to a direction parallel to the optical axis is completely conserved as propagating in free space.

Next, we derive PSF of the retrieved first GRF and the complex radiance function across the source plane. Let us assume a primary point source at $\boldsymbol{r}_s=(\boldsymbol{r}_{s\perp}, z_s)=(x_s, y_s, z_s)$. The cross-spectral density across the primary source plane is then represented by

$$\Omega^{(z_s)}(\boldsymbol{r}'_\perp, \boldsymbol{r}_\perp; \nu)=\Omega_0\delta^2\left(\frac{\boldsymbol{r}_\perp+\boldsymbol{r}'_\perp}{2}-\boldsymbol{r}_{s\perp}\right)\delta^2(\boldsymbol{r}_\perp-\boldsymbol{r}'_\perp), \tag{19}$$

where $\delta^2(\boldsymbol{r}_\perp)$ is the Dirac delta function and Ω_0 is a positive constant. The angular cross-spectral density across the source plane is obtained by taking the four-dimensional Fourier transform of $\Omega^{(z_s)}(\boldsymbol{r}'_\perp, \boldsymbol{r}_\perp; \nu)$:

$$\tilde{\Omega}^{(z_s)}(\boldsymbol{k}'_\perp, \boldsymbol{k}_\perp; \nu)=\frac{\Omega_0}{(2\pi)^2}\exp\left[-i(\boldsymbol{k}_\perp-\boldsymbol{k}'_\perp)\cdot\boldsymbol{r}_{s\perp}\right]. \quad (20)$$

Hence, the angular cross-spectral density of the source field is represented as[18]

$$\begin{aligned}\tilde{W}^{(z_s)}(\boldsymbol{k}'_\perp, \boldsymbol{k}_\perp; \nu)&=\frac{(2\pi)^2}{k_z k'_z}\tilde{\Omega}^{(z_s)}(\boldsymbol{k}'_\perp, \boldsymbol{k}_\perp; \nu)\\&=\frac{\Omega_0}{k_z k'_z}\exp\left[-i(\boldsymbol{k}_\perp-\boldsymbol{k}'_\perp)\cdot\boldsymbol{r}_{s\perp}\right]. \quad (21)\end{aligned}$$

The angular cross-spectral density across the observation plane can be written as a product of $\tilde{W}^{(z_s)}(\boldsymbol{k}'_\perp, \boldsymbol{k}_\perp; \nu)$ and the propagation kernel based on Eq. (9) as

$$\begin{aligned}\tilde{W}^{(0)}(\boldsymbol{k}'_\perp, \boldsymbol{k}_\perp; \nu)&=\exp\left[i(k_z-k'_z)z_s\right]\tilde{W}^{(z_s)}(\boldsymbol{k}'_\perp, \boldsymbol{k}_\perp; \nu)\\&=\frac{\Omega_0}{k_z k'_z}\exp\left[i(k_z z_s-\boldsymbol{k}_\perp\cdot\boldsymbol{r}_{s\perp})\right.\\&\qquad\left.-i(k'_z z_s-\boldsymbol{k}'_\perp\cdot\boldsymbol{r}_{s\perp})\right]. \quad (22)\end{aligned}$$

Taking the four-dimensional inverse Fourier transform of $\tilde{W}^{(0)}(\boldsymbol{k}'_\perp, \boldsymbol{k}_\perp; \nu)$ yields the cross-spectral density across the observation plane:

$$\begin{aligned}W^{(0)}(\boldsymbol{r}'_\perp, \boldsymbol{r}_\perp; \nu)&=\frac{1}{(2\pi)^2}\iiiint_{-\infty}^{\infty}\tilde{W}^{(0)}(\boldsymbol{k}'_\perp, \boldsymbol{k}_\perp; \nu)\\&\qquad\times\exp\left[i(\boldsymbol{k}_\perp\cdot\boldsymbol{r}_\perp-\boldsymbol{k}'_\perp\cdot\boldsymbol{r}'_\perp)\right]d^2k_\perp d^2k'_\perp\\&=\Omega_0 f^*(\boldsymbol{r}'_\perp-\boldsymbol{r}_{s\perp})f(\boldsymbol{r}_\perp-\boldsymbol{r}_{s\perp}), \quad (23)\end{aligned}$$

where

$$f(\boldsymbol{r}_\perp)=\iint_{-\infty}^{\infty}\frac{1}{2\pi|k_z|}\exp\left[i(k_z z_s+\boldsymbol{k}_\perp\cdot\boldsymbol{r}_\perp)\right]d^2k_\perp. \quad (24)$$

Let us now use a paraxial approximation with respect to k_z and k'_z derived by the Tailor series:

$$k_z\simeq -k+\frac{\boldsymbol{k}_\perp^2}{2k}, \quad (25)$$

then $f(\boldsymbol{r}_\perp)$ is written as

$$f(\boldsymbol{r}_\perp)\simeq\frac{i}{z_s}\exp(-ikz_s)\exp\left(-\frac{ik}{2z_s}\boldsymbol{r}_\perp^2\right). \quad (26)$$

On substituting Eq. (26) into Eq. (23), the cross-spectral density across the observation plane is rewritten as

$$\begin{aligned}&W^{(0)}(\boldsymbol{r}'_\perp, \boldsymbol{r}_\perp; \nu)\\&=\frac{\Omega_0}{z_s^2}\exp\left\{\frac{ik}{2z_s}\left[(\boldsymbol{r}'_\perp-\boldsymbol{r}_{s\perp})^2-(\boldsymbol{r}_\perp-\boldsymbol{r}_{s\perp})^2\right]\right\}. \quad (27)\end{aligned}$$

In a practical measurement of the cross-spectral density, the range of $\boldsymbol{r}_\perp$ and $\boldsymbol{r}'_\perp$ is limited by the linear dimension of a photodetector array. Therefore, the measured cross-spectral density is represented by a product of $W^{(0)}(\boldsymbol{r}'_\perp, \boldsymbol{r}_\perp; \nu)$ and the transmission function $A(\boldsymbol{r}_\perp)$ as

$$W_{\mathrm{m}}^{(0)}(\boldsymbol{r}'_\perp, \boldsymbol{r}_\perp; \nu)=A(\boldsymbol{r}'_\perp)W^{(0)}(\boldsymbol{r}'_\perp, \boldsymbol{r}_\perp; \nu)A(\boldsymbol{r}_\perp). \quad (28)$$

Note that $A(\boldsymbol{r}_\perp)$ is a real function and takes 1 in the measurement area and 0 outside. The four-dimensional Fourier transform of the measured cross-spectral density is then represented by

$$\begin{aligned}&\tilde{W}_{\mathrm{m}}^{(0)}(\boldsymbol{k}'_\perp, \boldsymbol{k}_\perp; \nu)\\&\quad=\frac{\Omega_0}{(2\pi z_s)^2}\iiiint_{-\infty}^{\infty}A(\boldsymbol{r}_\perp)A(\boldsymbol{r}'_\perp)\\&\qquad\times\exp\left\{\frac{ik}{2z_s}\left[(\boldsymbol{r}'_\perp-\boldsymbol{r}_{s\perp})^2-(\boldsymbol{r}_\perp-\boldsymbol{r}_{s\perp})^2\right]\right\}\\&\qquad\times\exp\left[-i(\boldsymbol{k}_\perp\cdot\boldsymbol{r}_\perp-\boldsymbol{k}'_\perp\cdot\boldsymbol{r}'_\perp)\right]d^2r_\perp d^2r'_\perp. \quad (29)\end{aligned}$$

Making the paraxial approximation shown in Eq. (25), the first GRF and the complex radiance function are represented by

$$\begin{aligned}&B_{\mathrm{1st}}^{(z)}(\boldsymbol{r}_\perp, \boldsymbol{s}; \nu)\\&\quad=|s_z|\left(\frac{k}{2\pi}\right)^2\iint_{-\infty}^{\infty}\tilde{W}^{(0)}(\boldsymbol{k}_\perp-\boldsymbol{q}_\perp/2, \boldsymbol{k}_\perp+\boldsymbol{q}_\perp/2; \nu)\\&\qquad\times\exp\left[i\boldsymbol{q}_\perp\cdot(\boldsymbol{r}_\perp-\boldsymbol{s}_\perp z)\right]d^2q_\perp, \quad (30)\end{aligned}$$

and

$$\begin{aligned}&B_{\mathrm{c}}^{(z)}(\boldsymbol{r}_\perp, \boldsymbol{s}; \nu)\\&\quad=|s_z|\left(\frac{k}{2\pi}\right)^2\iint_{-\infty}^{\infty}\tilde{W}^{(0)}(\boldsymbol{k}_\perp-\boldsymbol{q}_\perp, \boldsymbol{k}_\perp; \nu)\\&\qquad\times\exp\left[i\boldsymbol{q}_\perp\cdot(\boldsymbol{r}_\perp-\boldsymbol{s}_\perp z)\right]\\&\qquad\times\exp\left\{\frac{iz}{2k}\left[\boldsymbol{q}_\perp^2+(\boldsymbol{s}_\perp\cdot\boldsymbol{q}_\perp)^2\right]\right\}d^2q_\perp. \quad (31)\end{aligned}$$

As a simple example, let us assume that the source is located at $(x_s, 0, z_s)$ and that the cross-spectral density along only the x axis is measured within a baseline length of D. The transmission function is then represented by

$$A(\boldsymbol{r}_\perp)=\mathrm{rect}\left(\frac{x}{D}\right)\delta(y). \quad (32)$$

To derive PSFs of the first GRF and the complex radiance function, we set $z=z_s$ in Eqs. (30) and (31). Moreover, we consider the first GRF and the complex radiance function with respect to the fixed direction $\boldsymbol{s}=(0, 0, -1)$ for simplicity. Under these circumstances, we obtain the PSF of the first GRF over the source plane by substituting Eqs. (29) and (32) into Eq. (30) as follows:

$$\begin{aligned}B_{\mathrm{1st,m}}^{(z_s)}(x, 0)&=\frac{\Omega_0 D}{2}\left(\frac{k}{\pi z_s}\right)^2\mathrm{rect}\left(\frac{x}{D}\right)\\&\quad\times\frac{\sin\left\{\frac{k}{z_s}(D-2|x|)[x-x_s]\right\}}{\frac{kD}{z_s}[x-x_s]}, \quad (33)\end{aligned}$$

and the PSF of the complex radiance function is similarly derived by substituting Eqs. (29) and (32) into Eq. (31) as

$$\begin{aligned}&B_{\mathrm{c,m}}^{(z_s)}(x, 0)\\&\quad=\Omega_0\left(\frac{k}{2\pi z_s}\right)^{5/2}\exp\left(\frac{i\pi}{4}\right)\left[F(\alpha^{(+)})-F(\alpha^{(-)})\right]\end{aligned}$$

$$\times \exp\left[-\frac{ik}{2z_s}(x^2-x_s^2)\right]\operatorname{sinc}\left[\frac{kD}{2z_s}(x-x_s)\right] \qquad (34)$$

where

$$F(\alpha)=\frac{1}{1-i}\int_{-\infty}^{\alpha}\exp\left(-\frac{i\pi\tau^2}{2}\right)d\tau, \qquad (35)$$

and

$$\alpha^{(\pm)}=\sqrt{\frac{k}{\pi z_s}}\left(\pm\frac{D}{2}-x_s\right). \qquad (36)$$

Based on Eqs. (33) and (34), profiles of PSFs of the first GRF, the real part, and the magnitude of the complex radiance function are plotted in Fig. 2(a), (b), and (c), respectively, for source locations of $x_s=0$ mm, 0.3 mm, and 0.6 mm. Other parameters used are $k=9{,}929$ rad/mm, $D=2.4$ mm, and $z_s=110$ mm. Each power is normalized by the peak of the first PSF for $x_s=0$, namely, in the case that the point source is located on the optical axis. As seen from Fig. 2(a), the peak of the PSF of the first GRF lowers and the width broadens as the source location moves away from the optical axis. When the point source is located apart from the optical axis, the period of oscillation is asymmetric to the peak of the PSF, and oscillation of the left side of the peak is faster than that of the right side. In contrast, widths of PSFs of the real part and the magnitude of the complex radiance function are almost unchanged when the source moves. Height differences of PSFs shown in Figs. 2(b) and (c) are caused by the Fresnel integral term $F(\alpha^{(+)})-F(\alpha^{(-)})$.

Next, let us confine ourselves to the resolution power along the x axis. The full width at half maxima of PSFs of the first GRF, the real part, and the magnitude of the complex radiance function for $x_s=0$ mm are, respectively, 0.0175 mm, 0.035 mm, and 0.035 mm under the same conditions as Fig. 2. This means that the resolution power of the first GRF along the x axis is the highest in those of three radiance functions for an object on the optical axis. However, PSF of the first GRF broadens as the source location shifts away from the optical axis as stated above, whereas the width of PSF of the magnitude of the complex radiance function is invariant within the paraxial area. The width in the PSF of the real part of the complex radiance function changes somewhat owing to the quadratic phase term.

3. Numerical Calculation

Based on the mathematical formulation stated in Sect. 2, we will show the numerical examples of the retrieved radiance functions for a particular case. Assumed coordinate system and geometry are the same as those shown in Fig. 1. We assume quasi-monochromatic, spatially incoherent planar sources in a source plane located at $z=z_s=100{,}000$ mm (100 m). The intensity distribution across the source plane is binary as shown in Fig. 3(a). A region 2.4 mm square within the source plane is considered, and radiance distributions are calculated over the same area. The wavelength of light is assumed to be 632.8 nm.

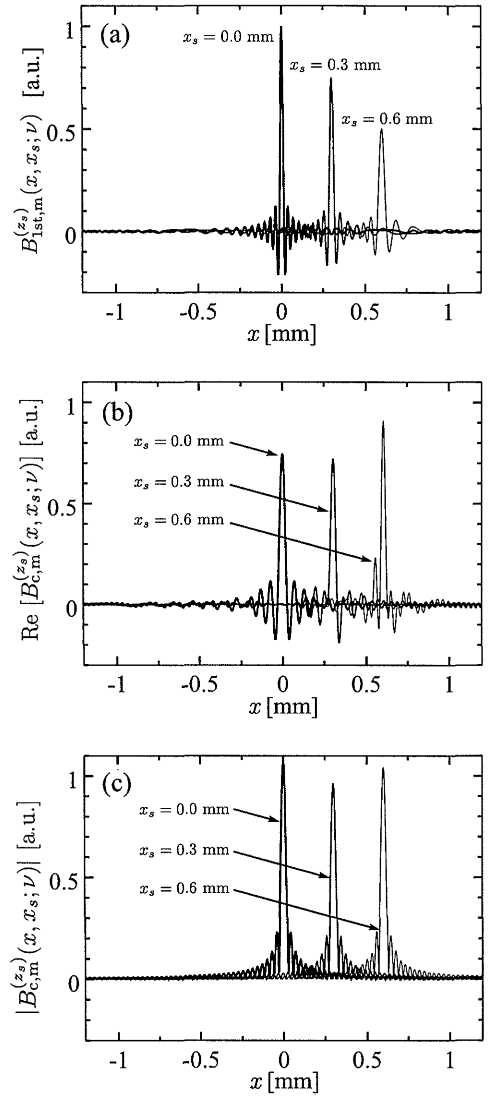

Fig. 2. PSFs of (a) the first GRF, (b) the real part of the complex radiance function for the source location $s_x=0$ mm, 0.3 mm, and 0.6 mm, and (c) the magnitude of the complex radiance function for the same s_x's as (b).

As a beginning, the first GRF and the real part of the complex radiance function for fixed $\boldsymbol{s}$'s across the observation plane are calculated under these circumstances, and the results are shown in Figs. 3(b) and (c). Since gray-levels are normalized by each maximum and minimum of the calculated radiance functions, the zero-levels differ. The direction $\boldsymbol{s}$, which specifies the direction of the considered plane wave, for the first GRF is set to $(1/2, 0, -\sqrt{3}/2)$, namely, the angle between $\boldsymbol{s}$ and the optical axis is 30° on the x–z plane. Remember that the first GRF for $\boldsymbol{s}=(0, 0, -1)$ is independent of the propagation distance, and the same image as the original source intensity will be obtained across any transverse planes. The direction of $\boldsymbol{s}$ for the complex radiance function is set to $(0, 0, -1)$. It is seen from Fig. 3(b) that the image

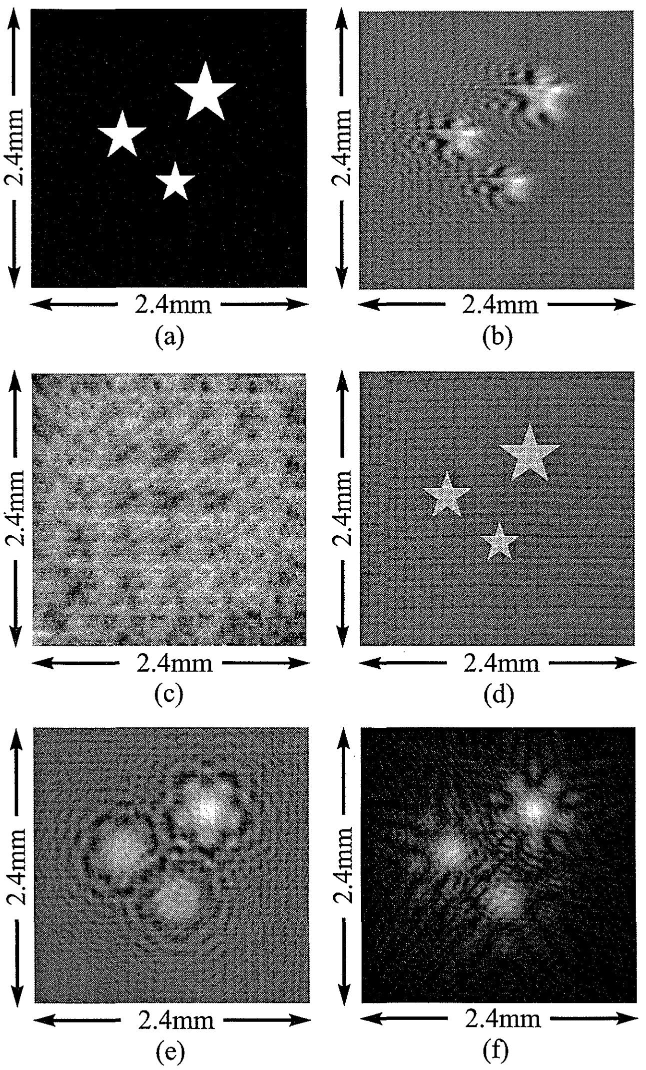

Fig. 3. (a) Intensity distribution of primary sources assumed for the computer simulation. (b) Spatial distribution of Walther's first definition of GRF 100,000 mm from the source plane and (c) the real part of the complex radiance function at the same distance as (b). (d) The first GRF 100 mm from the source plane, (e) the real part, and (f) the magnitude of the complex radiance function at the same distance as (d).

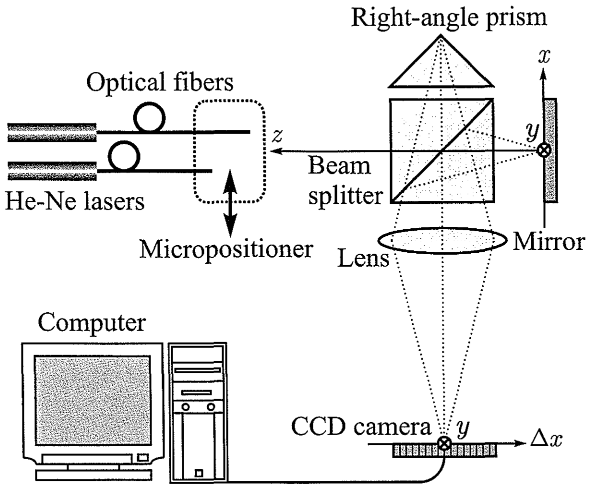

Fig. 4. Experimental setup for measuring the cross-spectral density.

retrieved as the first GRF exhibits shapes of three starred source with periodic oscillation that appears in the direction of $\boldsymbol{s}_\perp$. In contrast, the complex radiance function expands to the entire image.

Next, we inversely propagate the first GRF and the complex radiance function across the reference plane that is separated from the observation plane by 99,900 mm (99.9 m), that is 100 mm from the source plane. The retrieved images are shown in Figs. 3(d), (e), and (f). Figures 3(e) and (f) are, respectively, the real part and the magnitude of the complex radiance function. As seen from Fig. 3(d), the image retrieved as the first GRF almost coincides with the original source intensity though the contrast is lower than that of Fig. 3(a) because of minute oscillation around the edge of the sources. The complex radiance functions shown in Figs. 3(e) and (f) barely exhibit the three starred sources, but images are much blurred compared with the first GRF. The calculated results of radiance functions across the source plane are omitted because they are simply proportional to the source intensity as obvious from Eq. (18), although they were verified by simulation.

Differences between the first GRF and the complex radiance function imply the conservation characteristics of the radiance functions. As obvious from simulation results shown in this section, the conservation of the complex radiance function along $\boldsymbol{s}$ is much worse than that of the first GRF. In other words, the retrieved image as the complex radiance function is considerably blurred when $z \neq z_s$. The large angle between $\boldsymbol{s}$ and the optical axis makes the first GRF more blurred, but it may be impracticable to measure the cross-spectral density to retrieve the first GRF with an extremely large angle. For this reason, the complex radiance function is more useful than the first GRF for 3-D imaging.

4. Experimental Demonstration

In this section, we report the results of an experimental demonstration for retrieving the spatial distribution of the first GRF and the complex radiance function. The schematic of the optical setup is shown in Fig. 4. Although the x-y-z space is assumed in the general theory stated in Sect. 2, we measured the cross-spectral density along the x axis, and the GRF distributions on the x–z plane were retrieved for simplicity. Two optical fibers with core diameters of 8 μm each simulate two point sources. Tips of fibers are separated by 0.8 mm along the x axis and by 20 mm along the z axis. Since beams emitted from individual He–Ne lasers (wavelength 632.8 nm) are incident on each optical fiber, there is no correlation between the fields of the two point sources. A Michelson-type wave-front-folded interferometer consists of a beam-

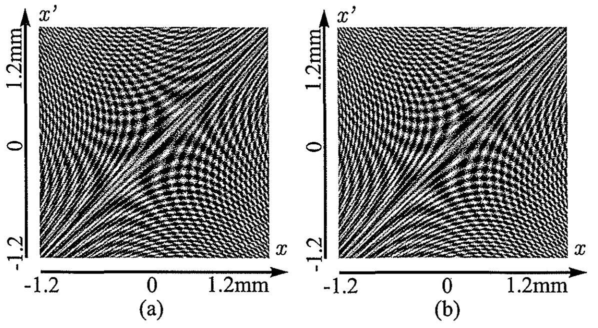

(a) (b)

Fig. 5. (a) Real and (b) imaginary parts of the measured cross-spectral density.

splitter, a right-angle prism, a mirror, an image forming lens, and a CCD camera. The right-angle prism on one path folds the wave front and the superposed beam is focused on the CCD camera by the image forming lens with a magnification factor of 1. In this experiment system, the observation plane in Fig. 1 corresponds to the mirror surface. The mirror is slightly tilted in order to introduce a carrier frequency into an interference fringe. The cross-spectral density along the y axis is regarded as uniform because the tips of optical fibers are located on the x–z plane and are sufficiently small. The cross-spectral density as a function of a two-point separation $\Delta x = x - x'$ for a specific average coordinate $\hat{x} = (x + x)/2$ is obtained by the Fourier analysis of the interference fringe. To measure the cross-spectral density with respect to all pairs of points within the observation baseline, the entire interferometer should be moved along the x axis. In the present experiment, the ends of the optical fibers that were fixed on a micropositioner were moved instead of the entire interferometer. Five hundred and twelve frames were recorded by the CCD camera and a computer while fibers moved 2.4 mm.

Real and imaginary parts of the measured cross-spectral density are shown in Figs. 5(a) and (b) as gray-level images. White represents a higher value. Horizontal and vertical axes represent the x- and x' axes, respectively, and a cross section along a diagonal line from top-right to bottom-left of the real part designates the intensity distribution over the observation axis. Taking the two-dimensional Fourier transform of the cross-spectral density with respect to x and x' gives the angular cross-spectral density as a function of k_x and k'_x. Using this angular cross-spectral density, we retrieve Walther's first GRF and the complex radiance function with respect to the fixed direction $\boldsymbol{s} = (0, 0, -1)$. The retrieved first GRF is plotted in Fig. 6 as a function of x. As pointed out in Sect. 2, the first GRF with $\boldsymbol{s}_\perp = (0, 0)$ is independent of the propagating distance z. Thus, two sharp peaks appear in the figure though the sources are located different distances from the observation plane. In other words, the first GRF with $\boldsymbol{s}_\perp = (0, 0)$ is conserved completely as it is propagating. It should be noted that the intensity distribution retrieved based on the van Cittert-Zernike theorem is given as a function of an angle seen from the observation point unless the source distance is known in advance, however, the two-point separation (0.8 mm, in this case) is obtained by the first GRF without the source distance.

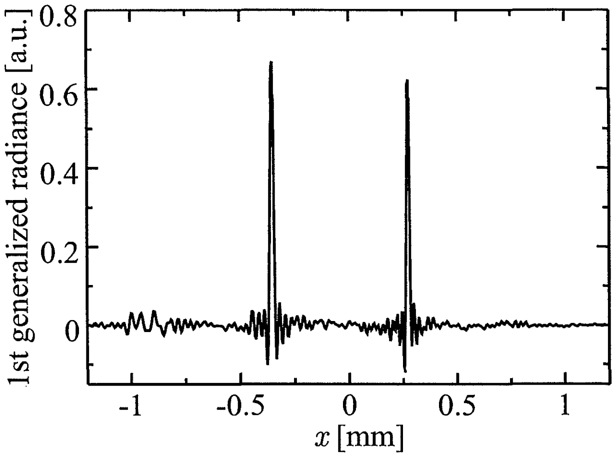

Fig. 6. Retrieved first GRF as a function of x.

Next, we show the retrieved complex radiance function. Unlike the first GRF, the complex radiance function depends on the propagating distance z. A sequence of spatial distributions of the complex radiance function along the x axis from $z = 0$ mm to $z = 200$ mm is calculated based on Eq. (13). The real part and the magnitude of the complex radiance function are shown in Figs. 7(a) and (b). Locations of two tips of optical fibers are retrieved almost exactly as higher values (white regions) in both figures. The cross sections of Figs. 7(a) and (b) at $z = 110$ mm and 130 mm, in which two point sources are located, are shown in Figs. 8(a), (b), (c), and (d). Sharp peaks in each graph represent focused sources. The oscillation appearing in Fig. 7(a) is reduced in Fig. 7(b), and it is also seen from Figs. 8(a), (b), (c), and (d). Although we suggested that 3-D imaging is possible by using the first GRF with respect to the direction $\boldsymbol{s}_\perp \neq (0, 0)$, the first GRF and the complex radiance function with $\boldsymbol{s}_\perp = (0, 0)$ were shown as experimental results. As seen from Eqs. (12) and (14), the first GRF is well conserved in the direction of $\boldsymbol{s}$. However, retrieving the first GRF with large $|\boldsymbol{s}_\perp|$ requires measuring the cross-spectral density with an extremely high spatial resolution to obtain a wide range of $\boldsymbol{k}_\perp$.

In our latest paper,[17] we proposed an interferometric 3-D imaging technique based on retrieving sequential cross-spectral densities within the considered slab geometry. This method can retrieve the intensity distribution on the 3-D space since the cross-spectral density with respect to the same point represents the spectral density, and this is proportional to the intensity as long as the source spectrum is quasi-monochromatic. We compared the processing time required for calculating the distribution of the complex radiance function and the inten-

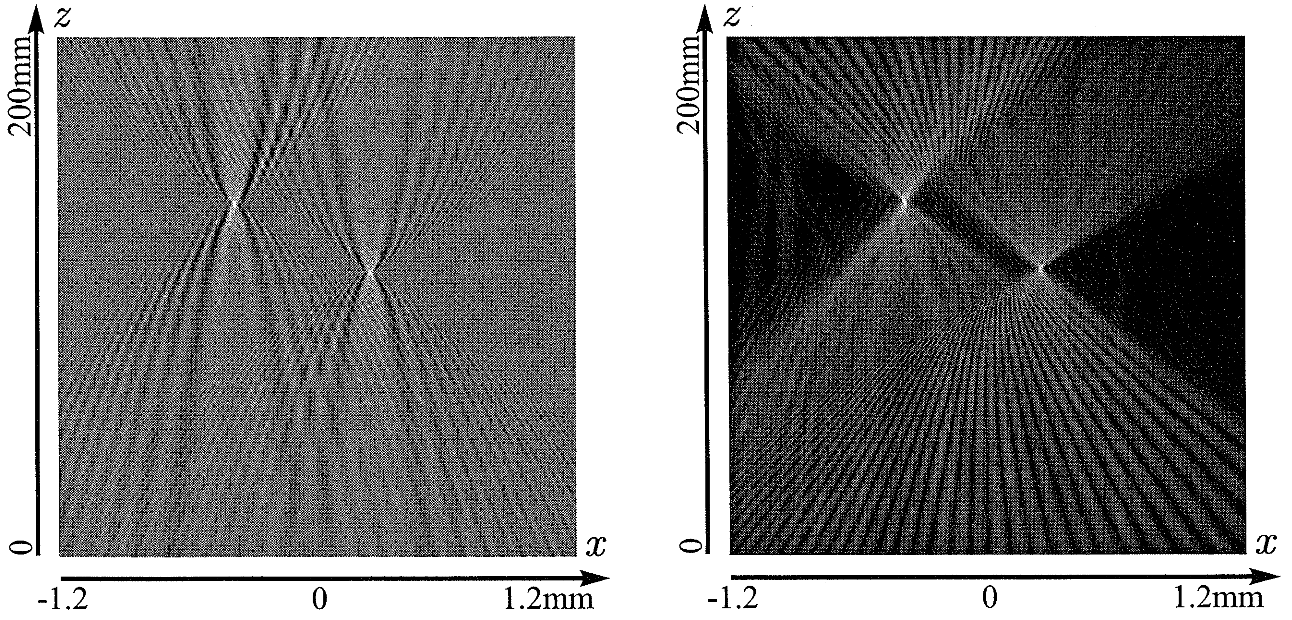

(a) (b)

Fig. 7. (a) Retrieved real part of the complex radiance function and (b) the magnitude of the complex radiance function on the x–z plane.

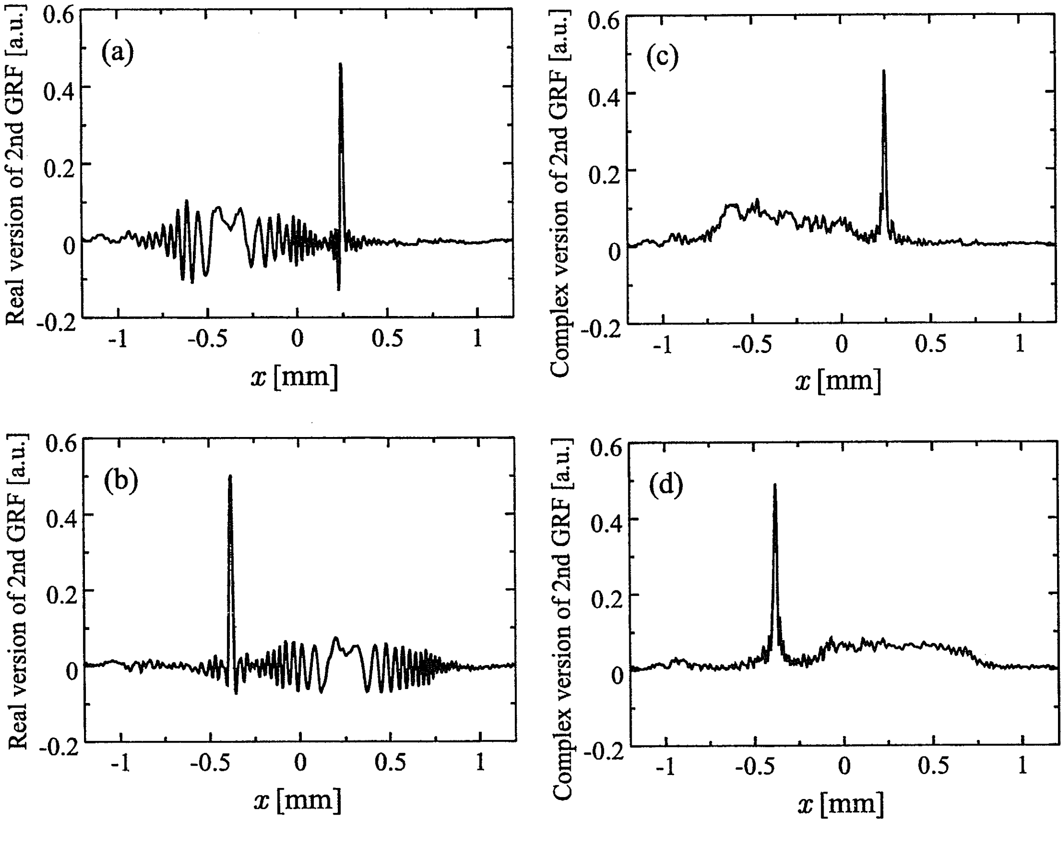

Fig. 8. Cross sections of the complex radiance function across source planes. (a) The real part at $z=110$ mm and (b) $z=130$ mm, and (c) the magnitude at $z=110$ mm and (d) $z=130$ mm.

sity distribution over the x–z plane. The distributions of the complex radiance function shown in Figs. 7(a) and (b) were calculated from the measured cross-spectral density shown in Fig. 5 in 8 seconds, while it took 3483 seconds to calculate the intensity distribution over the same slab geometry using a personal computer (CPU: Intel

PentiumII 450 MHz, OS: FreeBSD 2.2.8RELEASE). To retrieve sequential cross-spectral densities over the x–z space, the two-dimensional FFT and the two-dimensional inverse FFT must be performed at every z coordinate. In case of the present method, however, the two-dimensional FFT is required only once, and a radiance distribution at a particular z-coordinate is given by the one-dimensional FFT. Hence the processing time for these two methods differ greatly.

5. Conclusions

A new three-dimensional imaging technique based on retrieving Walther's first and second definitions of the generalized radiance function was proposed. The spatial distributions of these two types of generalized radiances can be calculated from the cross-spectral density propagated from primary sources in free space using the propagation law of the cross-spectral density described in the Fourier domain. An experimental demonstration of this imaging method was conducted by incorporating two uncorrelated point sources. The 3-D locations of sources were retrieved almost exactly as a spatial distribution of Walther's second definition of the generalized radiance. Walther's first definition of the generalized radiance showed the two point separation along the direction perpendicular to the optical axis. However, the longitudinal resolution is much worse than that of the second generalized radiance under the same conditions. Mathematical formulations of the proposed method were given and the point spread functions were also derived.

References

1) A. W. Lohmann, D. Mendlovic and G. Shabtay: J. Opt. Soc. Am. A **16** (1999) 359.
2) D. Mendlovic, G. Shabtay and A. W. Lohmann: Opt. Lett. **24** (1999) 361.
3) D. Mendlovic, G. Shabtay and A. W. Lohmann: Opt. Lett. **23** (1998) 1084.
4) H. Arimoto and Y. Ohtsuka: J. Opt. Soc. Am. A **15** (1997) 914.
5) F. Roddier: Phys. Rep. **170** (1998) 92.
6) D. L. Marks, R. A. Stack and D. J. Brady: Appl. Opt. **38** (1999) 1332.
7) H. Arimoto and Y. Ohtsuka: Opt. Lett. **23** (1998) 724.
8) P. Berio, D. Mourard, D. Bonneau, O. Chesneau, P. Stee, N. Thureau and F. Vakili: J. Opt. Soc. Am. A **16** (1999) 872.
9) J. W. Goodman: *Statistical Optics* (John Wiley & Sons, New York, 1985).
10) A. A. Michelson: *Studies in Optics* (University of Chicago Press, Chicago, 1962).
11) L. Mertz: *Transformations in Optics* (John Wiley & Sons, New York, 1965).
12) D. F. V. James, H. C. Kandpal and E. Wolf: Astrophys. J. **445** (1995) 406.
13) H. C. Kandpal, K. Saxena, D. S. Mehta, J. S. Vaishya and K. C. Joshi: J. Mod. Opt. **42** (1995) 447.
14) J. Rosen and A. Yariv: Opt. Lett. **21** (1996) 1011.
15) J. Rosen and A. Yariv: J. Opt. Soc. Am. A **13** (1996) 2091.
16) H. Arimoto, K. Yoshimori and K. Itoh: J. Opt. Soc. Am. A **16** (1999) 2447.
17) H. Arimoto, K. Yoshimori and K. Itoh: Opt. Commun. **170** (1999) 319.
18) E. Wolf and H. W. Carter: J. Opt. Soc. Am. **68** (1978) 953.
19) R. G. Littlejohn and R. Winston: J. Opt. Soc. Am. A **10** (1993) 2024.
20) K. Yoshimori and K. Itoh: J. Opt. Soc. Am. A **14** (1997) 3379.
21) A. T. Friberg: in *Summary of Research, SPIE Milestone Series, MS69*, eds. A. Friberg and B. Thompson (SPIE, Washington, 1993) pp. xv–xxxi.
22) A. Walther: J. Opt. Soc. Am. **58** (1968) 1256.
23) A. Walther: J. Opt. Soc. Am. **63** (1973) 1622.
24) L. Mandel and E. Wolf: *Optical Coherence and Quantum Optics* (Cambridge University Press, New York, 1995).